Study of dynamical properties in β-TCP/CH layers

A. Mina[a], J.C. Caicedo[a,*], and W. Aperador[b]
[a] *Tribology, Powder Metallurgy and Processing of Solid Recycled Research Group, Universidad del Valle, Cali-Colombia,*
[*] *Tel./Fax Number: 57+2+ 3122270 Ext 27*
e-mail: jcaicedoangulo1@gmail.com
[b] *Departament of Engineering, Universidad Militar Nueva Granada, Bogotá-Colombia.*

Received 20 August 2014; accepted 5 February 2015

β-Tricalcium phosphate/Chitosan (β-TCP/Ch) coatings were deposited on 316L stainless steel (316L SS) substrates by a cathodic electrodeposition technique at different coating compositions. The crystal lattice arrangements were analyzed by X-Ray diffraction (XRD), and the results indicated that the crystallographic structure of β-TCP was affected by the inclusion of the chitosan content. The changes in the surface morphology as a function of increasing chitosan in the coatings via scanning electron microscopy (SEM) and atomic force microscopy (AFM) showed the root-mean squares hardness of the β-TCP/Ch coatings decreased by further increasing chitosan percentage. The elastic-plastic characteristics of the coatings were determined by conducting nanoindentation test, indicating that the increase if chitosan percentage is directly related to increasing the hardness and elastic modulus of the β-TCP/Ch coatings. Tribological characterization was performed by scratch test and pin-on-disk test to analyze the changes in the surface wear the β-TCP/Ch coatings. Finally, the results indicated an improvement in the mechanical and tribological properties of the β-TCP/Ch coatings as a function of increasing of the chitosan percentage.

Keywords: Surfaces; monolayers; coatings; electrochemical techniques; hardness.

PACS: 68.47.Gh; 75.70.Ak; 68.35.Ct; 82.45.Bb; 62.20.Qp

1. Introduction

In biomaterials devices has been reported that after long term implantations, materials as stainless steel (316L SS) may potentially cause allergic reactions due to the release of nickel (Ni), molybdenum (Mo) and chromium (Cr) ions [1-3]. As an innovative strategy, surface modification of this class of metallic implants with ceramic coatings represents the most common solution to change the bulk properties of the metal substrate, and also improve the mechanical and tribological behavior of the surface into interface bone/implant [4-7]. In recent studies, hydroxyapatite (HA), compounds of HA and β-tricalcium phosphate (β-TCP), HA and chitosan and β-TCP and chitosan have been frequently examined as coating materials on metallic substrates for biomedical applications due to their favorable biocompatibility, mechanical, and tribological characteristics [8-10].

β-TCP coatings are the newest application trying to improve the biocompatibility of metallic implants [11-13]. On the other hand, chitosan is a natural cationic polysaccharide produced by *alkaline N-deacetylation* of chitin, a constituent of the *exoskeleton* from crabs and squid. It is widely used in biomedical applications due to its bioactive characteristics that promote cell proliferation [14]. The combination of β-TCP and chitosan as a bioactive compound can potentially improve the bone fixation and accelerate bone growth. So. The electrochemical deposition of biomaterials on metallic substrates has recently provided greater advantages in biomedical applications [2]. Many bioactive compounds that accelerate bone growth and improve bone fixation have been used as coating materials. The incorporation of these bioactive coatings to metallic implants represents great advances in the development of orthopedic devices. The coatings can be applied into the substrates by a variety of techniques, such as sputtering [15], thermal evaporation [16], chemical vapor deposition [17], spin coating [18], spray pyrolysis [19], sol-gel deposition [20] and electrochemical deposition [21]. The electrochemical deposition has superior advantages compare to other techniques due to its simplicity, low cost and room temperature operation [22]. Furthermore, electrochemical deposition of biomaterials can provide functionalized coating implants by modifying experimental solutions and conditions [23].

The time-dependent properties of β-TCP make it an ideal coating for implants, which supplies a temporary support for bone ingrowth, and eventually is replaced by natural tissue [24]. Among several clinical applications involving β-TCP, posterior spinal fusion and craniomaxillofacial applications have attracted considerable attentions [25]. Calcium phosphate-based bioceramics with improved mechanical properties and controlled resorbability can assist in designing optimal biodegradable bone substitutes for spinal fusion and craniomaxillofacial applications. The use of such bone implants also avoids the second surgery required for autograft harvesting [26].

The biomaterials depends on the surface characteristics that directly influence the biocompatibility by affecting the surface charge, surface topography, and etc. [27]. In addition, some mechanical and tribologial properties are also of importance (hardness and friction coefficient). For example, materials used as catheters need excellent tensile and mechanical characteristics. Therefore, both the biocompatibil-

ity and the mechanical properties of biomaterials need to be improved [28]. In this work, β-TCP/Ch coatings were deposited on the 316L SS substrates by using cathodic electrodeposition technique in order to obtain a possible functionalized coating implant. The influence of the chitosan percentage in the coating structures, which improved the mechanical and tribological response was characterized and discussed in current research. In this sense, the β-TCP/Ch coatings could be considered as promising materials for biomedical industry in temporal invasive prosthesis applications as they can effectively improve the bone/prosthesis interfaces.

2. Experimental details

The tricalcium phosphate, also known as β-$Ca_3(PO_4)_2$ or (β-TCP), and chitosan, also known as $((C_6H_{11}NO_4)_n)$ or (Poly-(1-4)-2-Amino-2-deoxy-β-D-Glucan) were used as material coatings. β-TCP-chitosan coatings β-TCP/Ch coatings were deposited via cathodic electro-deposition on AISI 316L SS substrates (12 mm of diameter and 5 mm of thickness). Electro-deposition technique was performed using the following conditions: current density of 260 mA, agitation velocity of 250 rpm, pH electrolyte of 10.4, and a temperature deposition of 60°C. The cylindrical 316L SS substrates were prepared by grinding to 600 grit water proof silicon carbide papers, then they were activated by superficial electrochemical etching using an acid solution of 1:1:1 HCl:H_2SO_4:H_2O, to improve the adhesion characteristics in the substrate-coating interfaces. Finally, the substrates were cleaned in an ultrasonic bath with acetone and rinsed in deionized water in order to remove the organic contaminants.

The electro-deposition process was performed using an electrolyte compound of two solutions. The first one was β-TCP dissolved in an ethanol-water 1:3 solution; and the second one was carried out with chitosan solution dissolved in acetic acid 2%. The structural characterization was performed by X-Ray diffraction (XRD) Bruker D8 Advance with Cu cathode and scintillation detector using the setup 0-20 and making a sweep of 20° to 80° with a step of 0.01 degrees and a time per step of 2 seconds with Cu Ka radiation ($\lambda = 1.5405$ Å). The diffraction patterns were obtained as a function of increase in the chitosan concentration from β-TCP/Ch coatings, these patterns were further analyzed to determinate the changes in the crystal lattice arrangements. In addition, the different lattice arrangements of coating were compared and the changes in preferential peaks were determinate due to the inclusion of chitosan. The increase of intensity as a function of chitosan weight percentage was determined after to be applied the full width at half maximum (FWHM) criterion for the XRD patterns [29]. The surface chemical characterization of the β-TCP-Ch coatings were performed using a scanning electron microscope (SEM) JEOLJSM-6490LV to determinate the different phases on the surface coating. Energy Dispersive X-Ray (EDX) analysis was carried out to investigate the distribution of the different elements in the composites and to evaluate the changes of chemical composition as a function of chitosan weight percentage.

Atomic Force Microscopy (AFM) was used for a quantitative study of the surface morphology in β-TCP/Ch coatings using an AFM Asylum Research $MFP-3D^{®}$ and calculated by a Scanning Probe Image Processor ($SPIP^{®}$), which is the standard program for processing and presenting AFM data. Therefore, this software has become the *de-facto* standard for image processing at the nanoscale. The mechanical properties were defined using a Nanoindentation test, by using a Nanoindenter Ubi1-Hysitron to obtain elastic-plastic properties of the coatings. A three-side Berkovich diamond indenter with a tip radious of about 100 nm was used. After nanoindentation measurements, the load-penetration depth curves were performed to calculate the hardness and elastic modulus through the Oliver-Pharr method [30]. Tribological characterization was developed with a Microtest, *MT 400 98* tribometer, using a 6-mm diameter 100Cr6 steel-ball-like counter body slide. The load applied was 5 N with a total running length of 1000 m (around 29000 cycles) and 0.10 m/s. Scratch test was used to evaluate the adhesion strength between the β-TCP/Ch coatings and the 316L SS substrates. This technique was performed with a scratching speed of 4 mm/min and a continuous load rate of 1 N/s. The scratch test was also used to calculate the critical load (Lc) as a function of chitosan percentage, and determine the cohesive failure of the coatings.

3. Results and discussion

3.1. XRD Results

To study of crystalline structure of the prepared β -TCP/Ch coatings, XRD technique was used to obtain the diffraction patterns of each coating. Figure 1 shows the diffraction patterns of β -TCP peaks at low angles, preferential orientations (0018), (1118) and (0502) for $2\theta =$ (43.55°, 47.06° and 50.68°), respectively. The results indicate that the preferential orientations, corresponding to the ceramic phase of the coating layers, are in agreement with the Joint Committee on Powder Diffraction Standards (JCPDS) [31]. Figure 1 also exhibits the changes in rhombohedral configurations of β-TCP as a function of chitosan percentage. From this figure, the compression stress was also identified due to the changes in the peak morphology with chitosan percentage increasing [31]. Moreover, the diffraction patterns show the influence between the peak intensity and the chemical composition for β-TCP/Ch coatings. In this study, a displacement and widening of the preferential peaks was observed for all the samples.

The diffraction patterns exposed in Fig. 1 show a variation in the intensity of the preferential peaks oriented (0018) at $2\theta = 43.6°$ as a function of chitosan percentage, which is in an agreement with the results reported by other authors [10,31]. The variations in XRD patterns were appreciated using the *full width at half maximum* (FWHM) criterion for the patterns. Therefore, the crystal structure deformation data

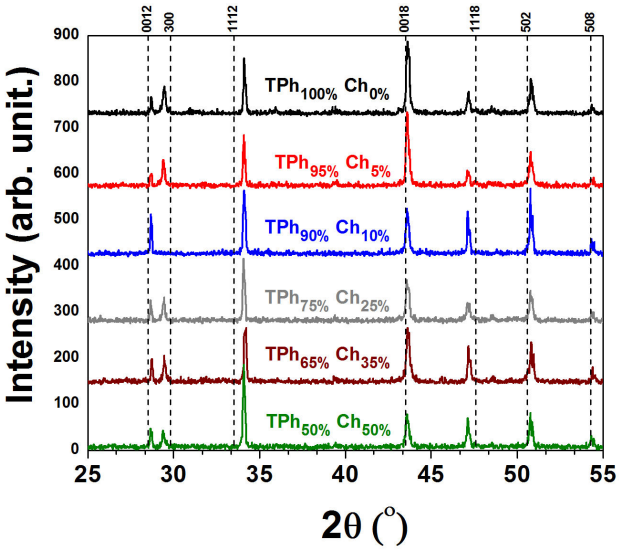

FIGURE 1. XRD patterns of β-TCP/Ch coatings deposited with different chemical compositions. The diffraction patterns show rhombohedral configurations corresponding to β-TCP and also a displacement and widening of the preferential peaks that indicate the compression stress due to the increase in the chitosan percentage.

suggests an inversely proportional relationship between the chitosan percentage and the peak intensity. Analyzing the diffraction patterns in Fig. 2 shows a variation in the intensity of the preferential peaks oriented (0018) at $2\theta = 43.6°$ as a function of chitosan percentage in the coatings.

The crystallographic behavior described above is shown in Fig. 2a where it is analyzed the shape and size variation associated to preferential peaks. Furthermore, the same shape and size variation as a function of chitosan percentage was observed in Fig. 2b. This figure also exhibits a decreasing in peak area and peak height for the preferential peak (0018) which can be contributed to the changes in the internal residual compression stress [10,23,31]. Consequently, it was possible to observe that the peak variation suggests an inverse relationship between the chitosan percentage and the peak intensity. The observation of this peak variation demonstrates a crystal structure deformation due to the compression stress applied by chitosan molecules in the β-TCP structure.

3.2. SEM analysis

To analyze the surface characteristics of different β-TCP/Ch coatings SEM was used. Figure 3 exhibits SEM micrographs of different coatings as a function of chemical compositions. The micrographs show the changes in the surface morphology as a function of chitosan percentage, which is in accordance with previous publications [10,30,32]. Therefore, Fig. 3a presents a fibrillar structure matrix associated to the β-TCP particles, this figure also demonstrated irregular dispersed particles associated to the particles which were not dissolved in the electrolyte solution deposited on the surface coating by ionic exchange from (Ca^{2+} and PO_4^{-3}).

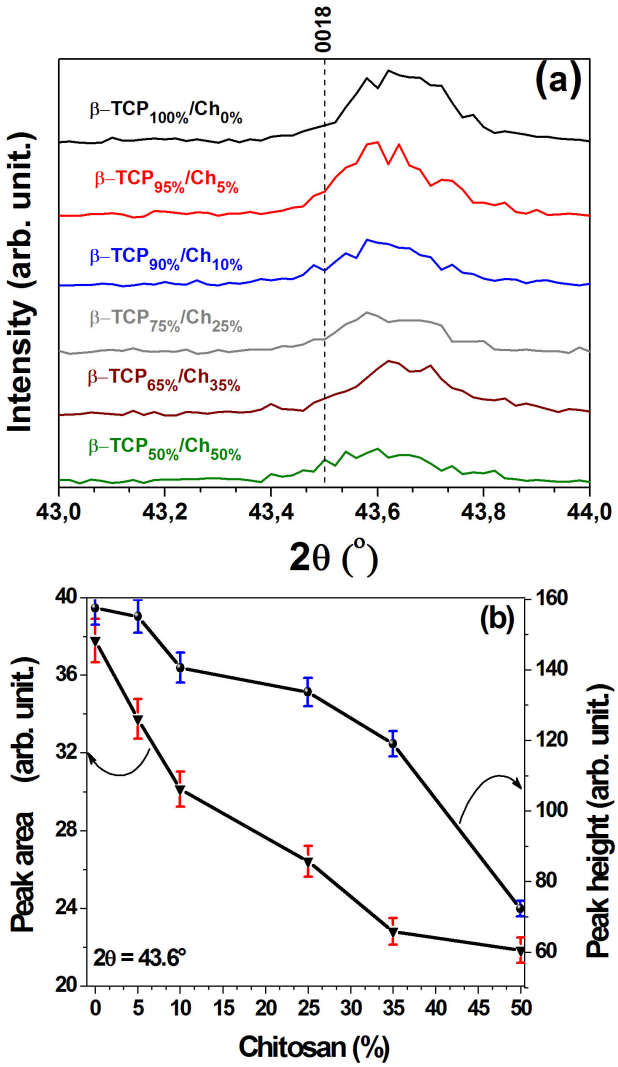

FIGURE 2. XRD patterns of different β-TCP/Ch coatings: (a) full width at half maximum (FWHM) variations as a function of chitosan percentage change and (b) peak area and peak height changes of preferential peak (0018) as a function of chitosan percentage. The curves show the compression stress effect in crystal structure due to the changes in chitosan percentage; it was evidenced by the decrease of peak area and peak height while the chitosan percentage increased.

Figure 3b exhibits the surface coating when it has 5% of chitosan, it showed that the number of particles increased associated with the polymerization of chitosan molecules which are not dissolved in the saturated electrolyte. Also, it was possible to observe that fibrillar structure matrix has disappeared, and it was replaced by a matrix with angular particles dispersed on the surface coating without defined orientation. This effect visually demonstrates the functionalization effects between the β-TCP particles and Ch molecules [24,26].

On the other hand, Fig. 3 shows that the thickness of the deposited particles decrease as a function of the increasing of chitosan percentage (Fig. 3b-e). Moreover, increasing of the chitosan percentage influences the deposited particles on the

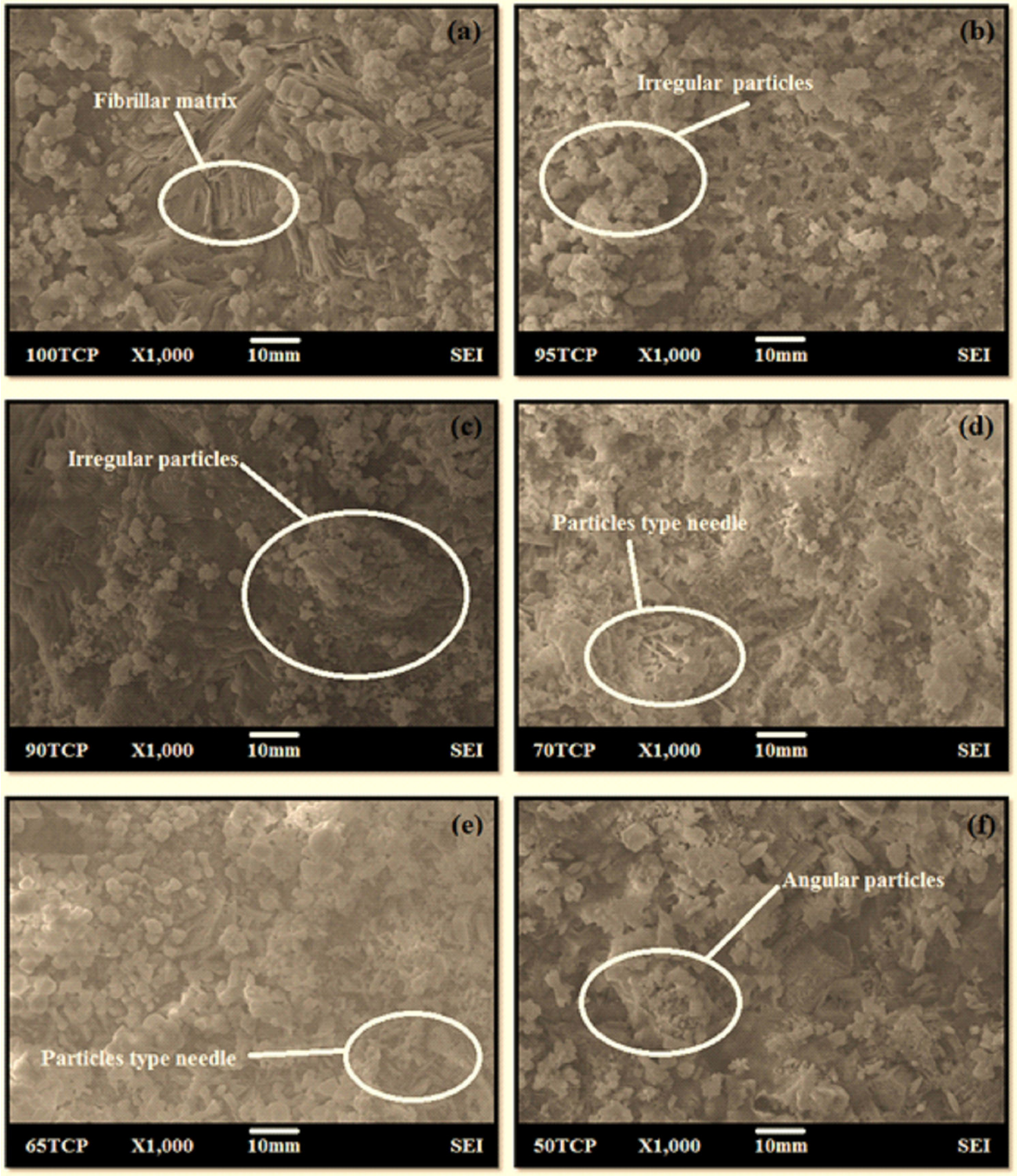

FIGURE 3. SEM micrographs of different β-TCP/Ch coatings: (a) β-$TCP_{100\%}/Ch_{0\%}$, (b) β-$TCP_{95\%}/Ch_{5\%}$, (c) β-$TCP_{90\%}/Ch_{10\%}$, (d) β-$TCP_{90\%}/Ch_{25\%}$, (e) β-$TCP_{65\%}/Ch_{35\%}$, and (f) β-$TCP_{50\%}/Ch_{50\%}$. The irregular particles are related with the particles without a defined shape; Particles type needle are elongated particles and angular particles are agglomerated particles with angular shapes.

surface to be thinner than the other coatings with lower chitosan percentage and presents an angular shape similar to needle shape.

Furthermore, these results exhibit progressive increase in the percentage and the size of particles deposited on the surface coating. The chitosan particles have a tendency to homogenize eliminating the surface area of the needle-like structure. In this way, Fig. 6f (a typical micrograph of surface coating with 50% of chitosan) shows a surface without needle-like structures, probably due to increasing of irregular particles.

Figure 3e shows a typical micrograph of the surface coating with 50% of chitosan, this micrograph presents a surface without needles structures probably due to the increasing of irregular particles observed in the last figures (Fig. 3b-e). Allotropic changes in the surface morphology of β - TCP/Ch

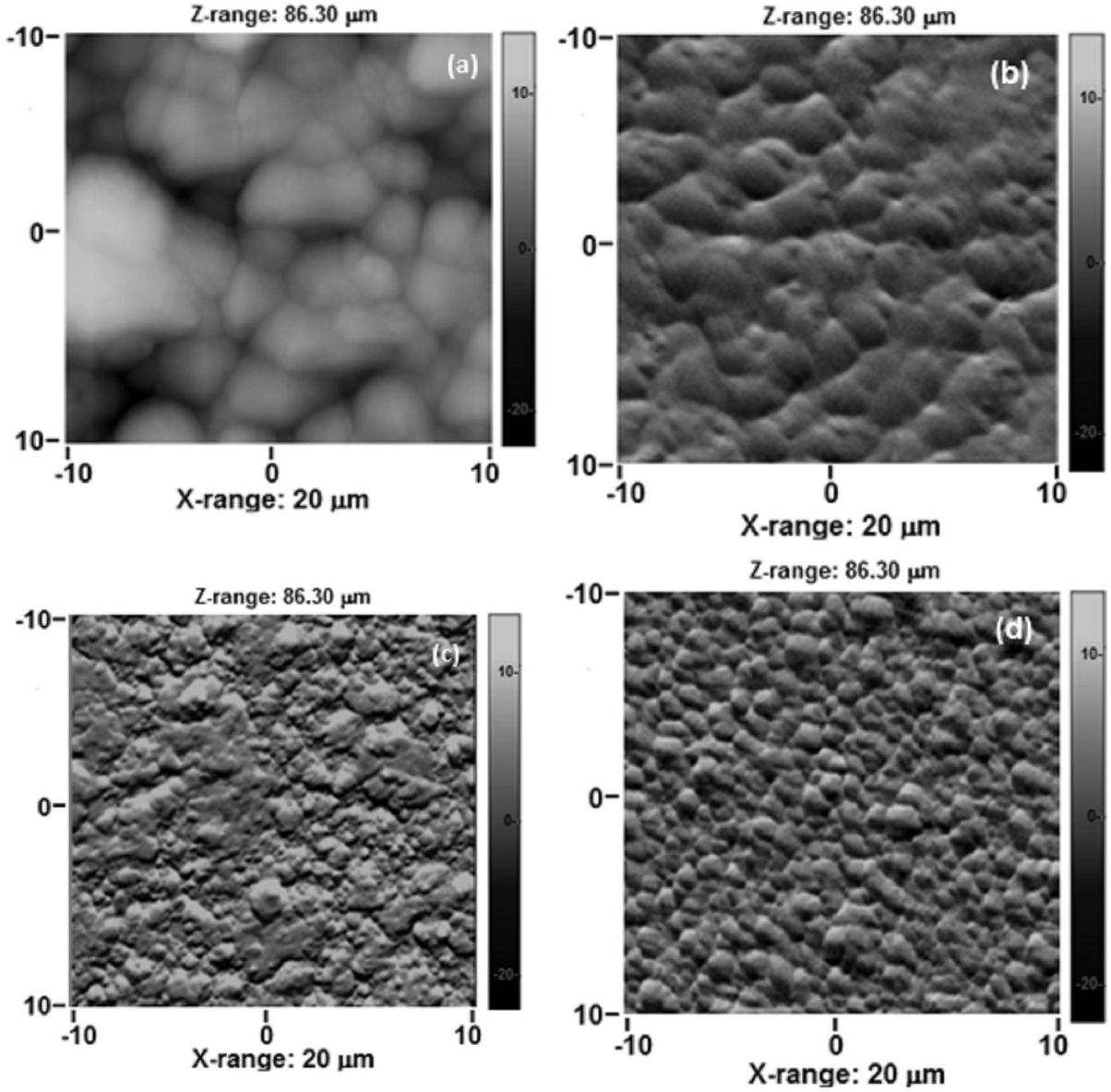

FIGURE 4. Representative AFM images of β-TCP/Ch coatings on the 316L SS substrates: (a) β-TCP$_{100\%}$/Ch$_{0\%}$; (b) β-TCP$_{95\%}$/Ch$_{5\%}$; (c) β-TCP$_{65\%}$/Ch$_{35\%}$; and (d) β-TCP$_{50\%}$/Ch$_{50\%}$ coatings.

coatings were described previously, which can be related to the changes in the crystallographic arrangement presented in the Fig. 1 and Fig. 2.

3.3. AFM analysis

AFM analysis was used to study the surface morphology of different β-TCP/Ch coatings. It is known that the surface morphology and roughness of coatings have a very important role on the final characteristics of the implants, since the reactions at the tissue/coating interface is directly related to the surface morphology. Taking this note into account, different β-TCP/Ch coatings as function of chitosan percentage were analyzed in an area of 20 μm $\times$ 20 m for each sample with a z-scale around 86.30 ± 2.0 μm.

The morphology and the root-mean-square roughness of the β-TCP/Ch coatings are shown in Fig. 4, it suggests that increasing the chitosan percentage can cause major changes in the surface topography and roughness. In this way, by increasing the chitosan percentage, the surface morphology changed and the surface roughness decreased.

The AFM micrograph showed in Fig. 4a was obtained from the β-TCP coating surface, which shows rounded particles overlapped between them, taking into account that the scale of measurements is a clear evidence that this coating is obtained from nanopowder. In addition, a qualitative analysis indicates that the sample contains predominantly particles of almost the same size and shape similar to the results reported by previous publications [33]. The allotropic changes in the surface morphology of the β-TCP/Ch coatings

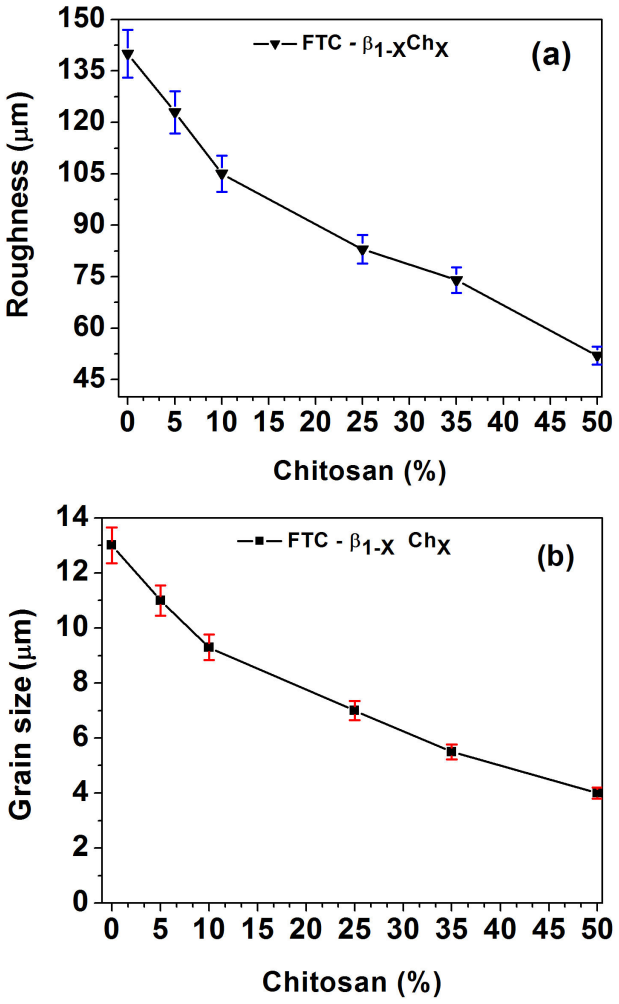

FIGURE 5. Morphological analysis of β-TCP/Ch coatings on the 316L SS substrates: (a) Roughness as a function of chitosan percentage curve, and (b) Grain size as a function chitosan percentage.

were described previously, indicating that these changes are related to the changing in the size and distribution of the particles. It is possible to infer that the changes in the crystallographic arrangement obtained by XRD analysis are related to the growth, size and distribution of the particles, at the same time the allotropic changes of the surface morphology is related to the changes in the surface topography observed by the SEM micrographs.

Applying statically analysis on AFM images using a Scanning Probe Image Procesor (SPIP®), it was possible to measure the morphological changes of the β-TCP/Ch coatings. Figure 5 shows the roughness and grain size trend as a function of chitosan percentage. Similar to the results from the SEM analysis it was possible to observe a decrease of coating roughness by further increasing the chitosan content. The previous published studies indicated that the values of grain size are closely related to the values of roughness, therefore, a decrease in the surface roughness implies a decrease in the grain size [34]. This effect is evidenced in Fig. 5 which

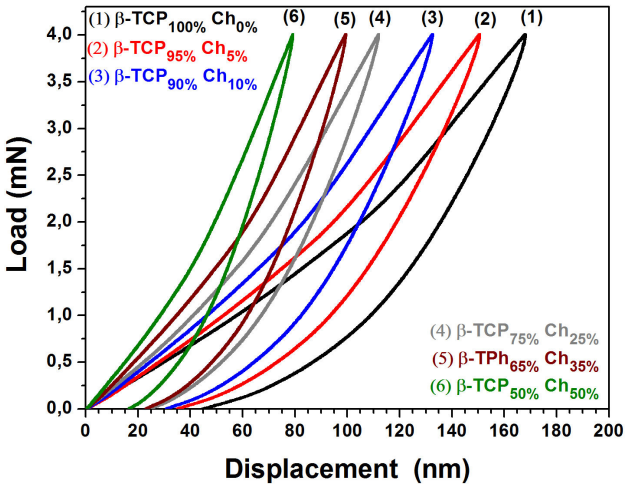

FIGURE 6. Nanoindentation test results for the β-TCP/Ch coatings: load-displacement indentation curves as a function of increasing the chitosan percentage.

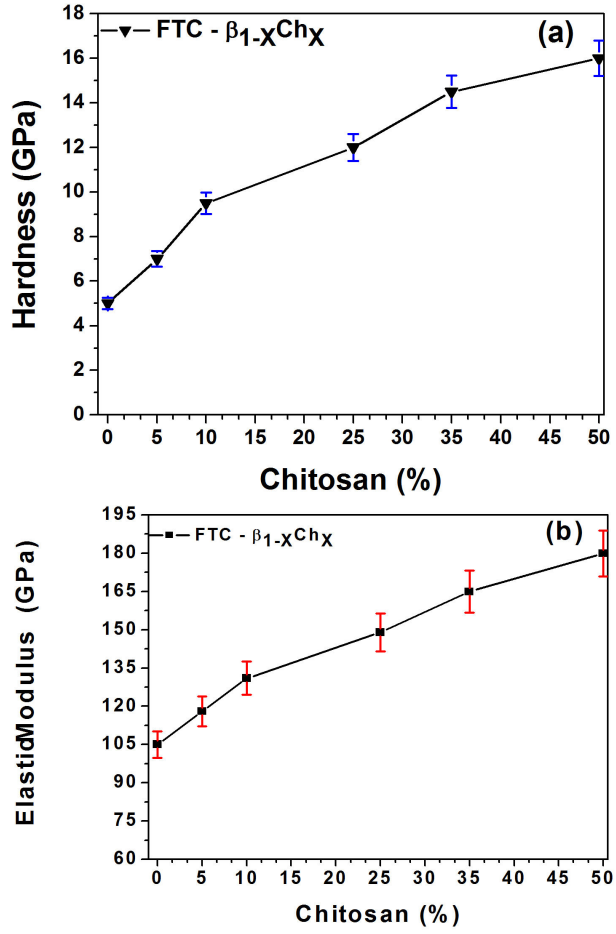

FIGURE 7. Mechanical properties of the β-TCP/Ch coatings: (a) Hardness values of the β-TCP/Ch coatings as a function of chitosan percentage and (b) Elastic modulus of the β-TCP/Ch coatings as a function of chitosan percentage.

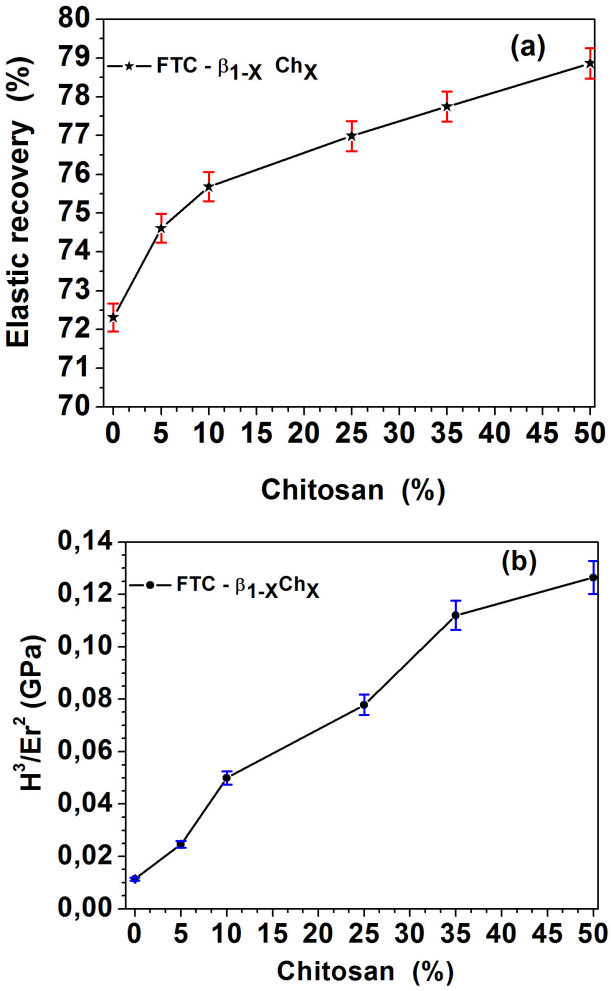

FIGURE 8. Mechanical properties: (a) Elastic recovery as a function of chitosan percentage, and (b) Plastic deformation resistance as a function of increasing in the chitosan percentage.

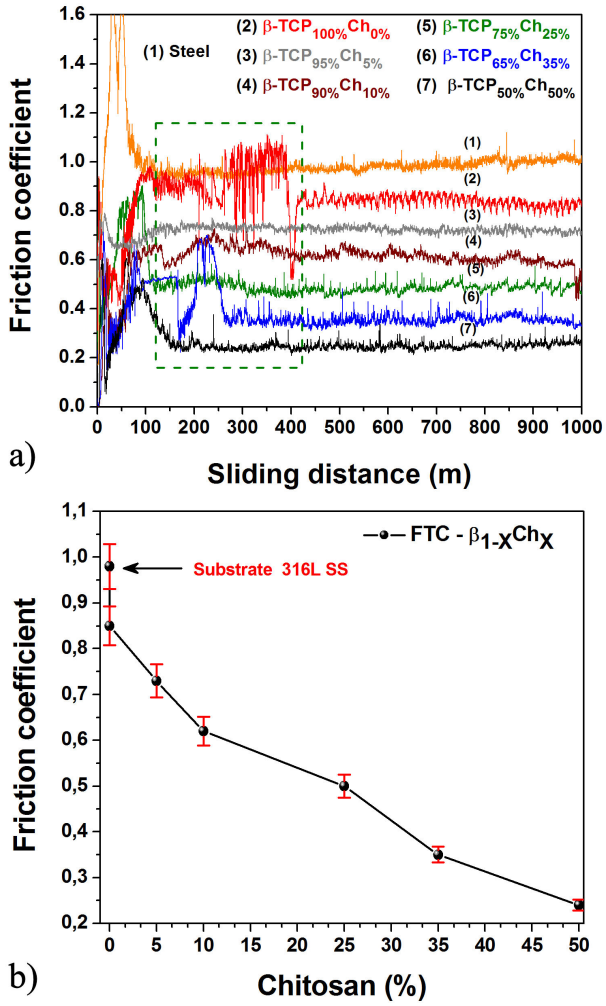

FIGURE 9. Tribological results of the 316L SS substrates coated with β-TCP/Ch coatings: (a) friction coefficient as a function of sliding distance, and (b) friction coefficient as a function of chitosan percentage. The curves explain an inversely proportional relationship between the chitosan amount and friction coefficient.

shows the decrease of roughness and grain size as a function of increasing of the chitosan amount. Finally, it is important to remark that the surface morphology results are related to the mechanical and tribological behavior. Therefore, the grain size reduction increases the toughness and hardness values. Also a smooth surface with a superficial homogeneity and low friction coefficient can help to increase the wear resistance [34,35].

3.4. Mechanical properties

The load-displacement indentation curves of the β-TCP/Ch coatings were obtained using the standard Berkovich indenter in a nanoindentation test. The load-displacement indentation as a function of chitosan percentage is shown in Fig. 6, which exhibits an elastic-plastic behavior of the coatings. The displacement of indenter at maximum load was analyzed for each coating. Figure 6 shows that the values of displacement decrease as a function of increase in the percentage of chitosan content. The lower values of displacement indicate an increase of penetration resistance, which implies a possible mechanical properties improvement.

The XRD patterns indicated that the compression stresses applied by chitosan inclusion in crystallographic structure of β-TCP associated with the deformation in the preferential peaks. This deformation in β-TCP structure suggest a kind of hardening by deformation due to a possible inclusion of chitosan in interstitial zones of β-TCP that can increase the value of the lattice parameter Burgers vector (this can produce a hardening). In this way, the improvement in mechanical properties could be related to the structural changes occurring by inclusion and increase of chitosan in the crystallographic arrangement of β-TCP.

Moreover others hardening mechanism can be used to explain the increase in the mechanical properties, but apparently no increase in dislocation density occurs to explain this. Then, it is possible that mechanical properties rises due to a "solid solution" mechanism or by a lower grain size as quitosan increases.

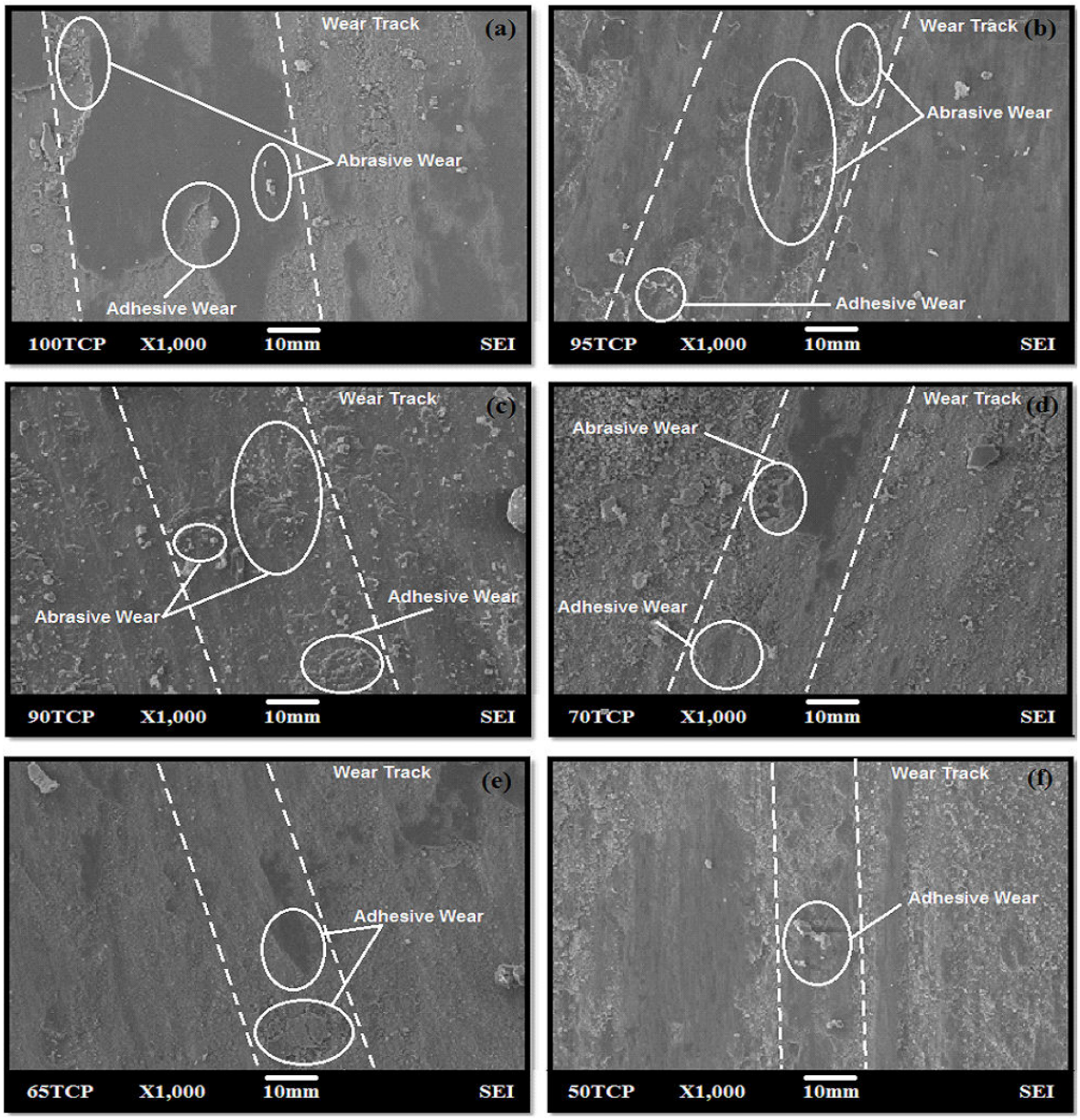

FIGURE 10. SEM micrographs for the wear tracks, evidencing the changes in the wear mechanism (abrasive y adhesive wear) as a function of chitosan percentage for all the β-TCP/Ch coatings

It was possible to determinate the values of hardness (H) and elasticity modulus (Er) using the indentation method developed by Oliver and Pharr [36]. Figure 7a shows an increase of hardness while increase the chitosan percentage by using Eq. (1) (which relate hardness with the ratio between maximum applied load and contact area).

$$H = \frac{p_{\max}}{A(h_c)} \tag{1}$$

where $P_{\max}$ is the maximum applied load and $A(hc)$ is the area associated to the surface where the load is applied. This equation is according with [30,36]. Figure 7 shows the increasing of mechanical properties as a function of chitosan percentage. As mentioned before, this increase of *Er* and H could be related with little changes in the crystallography orientation observed in the XRD patterns (Fig. 1) associated to the changes in the area and height of the central peak.

Hajek and co-workers [37] proposed an expression to calculate the elastic recovery for the coatings. In this research, Fig. 8 shows the plastic deformation resistance (H^3/Er^2) and elastic recovery (R). The obtained results here are in agreement with other authors [38-42]. The elastic recovery for the β-TCP/Ch coatings was calculated by using the following Eq. (2) [36].

$$R = \frac{\delta_{\max} - \delta_p}{\delta_{\max}} \tag{2}$$

where $\delta_{\max}$ is the maximum displacement and δ_p is the residual or plastic displacement. The equation data was taken

from the load-penetration depth curves of indentations for each coating according to the results obtained from nanoindentation test and exhibited in Fig. 6. The best mechanical properties were reached by the coating with the highest amount of chitosan content. Figure 8 shows an inverse proportional relation between the mechanical properties and chitosan percentage. In this sense it was possible to observe that the elastic recovery and plastic deformation resistance values increase as a function of chitosan amount increase, similar to the results analyzed in elastic modulus and hardness.

From the load-displacement curves Fig. 6 its shows that the increase of the elastic recovery (Fig. 8) corresponds to a reduction of the plasticity (or plastic deformation), therefore, it was reflected an increase in the Elastic modulus (Fig. 7), which could be interpreted as a hardening of β-TCP/Ch compound with increasing the addition of chitosan.

3.5. Tribological properties

The friction coefficient values were obtained from pin-on-disk test, in this way, the tribological properties were analyzed into tribological pair between the 316L SS substrate and β-TCP/Ch coatings system and a 100Cr6 steel balls. Figure 9a shows the friction coefficient as a function of sliding distance for the substrate and coatings. The curves displayed in Fig. 9a showed two different stages; the first stage is called the running-in period, where the friction coefficient began at low levels; due to an interferential friction mechanism it is caused by few contacts between the steel ball and the coating surface through the roughness tips in both counterparts. As slide distance increase, the friction coefficients increase too due to the formation of wear debris by cracking of roughness tips on both counterparts according to the tribological model proposed by Archard [43]. The second stage, also called steady state is a zone of the curve where the roughness of tribological pair is smoothed and the friction coefficient value is stabilized. In this stage, the surface coatings are molded by the surface of a 100Cr6 steel ball, since the ball surface is harder than the coating surface. Finally, it is possible to suppose that the friction coefficients are closely related to the slide distance, and by increasing the slide distance, the friction coefficient decreases [44,45].

A good combination between elastic-plastic properties (*H, Er*) and surface properties (*Ra*) could possibly guarantee a good tribological response. In fact, the tribological properties depend mainly on the elastic-plastic properties, thus, while the chitosan percentage increases H and Er, the roughness decreases. Therefore, the values of friction coefficient decrease as is shown in Fig. 9b. As it was explained above the chitosan amount and friction are closely related, so Fig. 9b shows the friction coefficient as a function of chitosan percentage increase curve, this curve shows that μ decreases when the chitosan percentage increases.

3.5.1. *Wear analysis*

After a sliding distance of 1000 m in the pin-on-disk tests, SEM analysis was used to evaluate the wear properties of the surfaces. Figure 10 shows the micrographs of the surface wear for all the coating samples at 1000X and their wear mechanism, demonstrating a continuous and smooth wear track, with a depth below the film thickness. Therefore, the abrasive wear is presented in each micrograph, which is related to the generation of loose wear debris corresponding to rupture, cohesive failure and delamination of the coatings due to the interaction between the slider pair (steel ball) and the

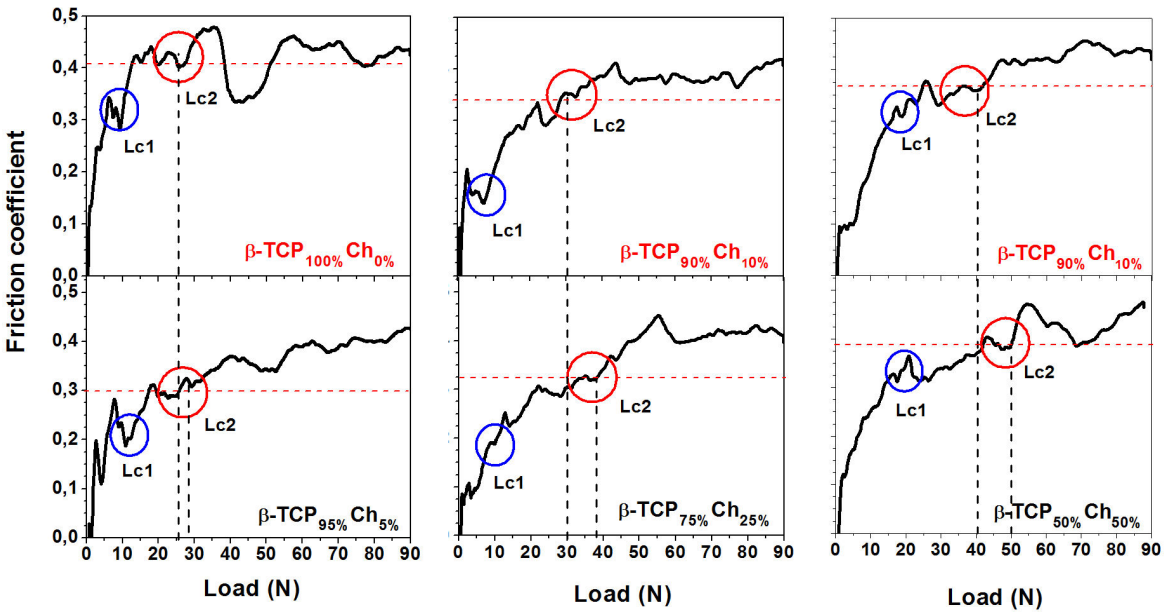

FIGURE 11. Tribological results for the friction coefficient curves versus the applied load; showing the cohesive (L_{C1}) and adhesive (L_{C2}) failure mode for the β-TCP/Ch coatings as a function of increasing in the chitosan percentage.

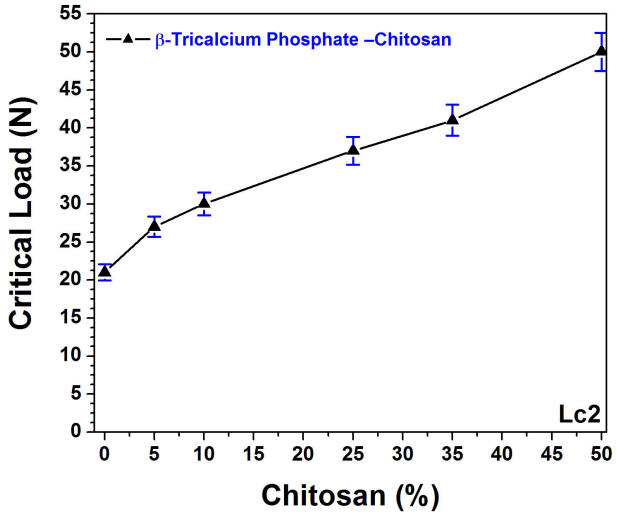

FIGURE 12. Critical load associated to the adhesion failure (L_{c2}) as a function of chitosan percentage for all the coatings: (β-$TCP_{100\%}$/$Ch_{0\%}$, β-$TCP_{95\%}$/$Ch_{5\%}$, β-$TCP_{90\%}$/$Ch_{10\%}$, β-$TCP_{90\%}$/$Ch_{25\%}$, β-$TCP_{65\%}$/$Ch_{35\%}$, and β-$TCP_{50\%}$/$Ch_{50\%}$..

β-TCP/Ch coating surfaces. Thus, the wear debris interact again with both surfaces, generating grooves and scratches on the coating surfaces. In this sense, high friction coefficient, and other wear mechanisms associated with the mechanical fatigue due to cyclical charges of pin on the surface is evidenced by cracks. Figure 10a-f clearly show the effects of chitosan percentages on the wear mechanism of the coatings. Therefore, it can be concluded that by increasing the chitosan percentage, a decrease in the trace of abrasive particles and cracks could be observed. The decreasing of the wear mechanism (adhesive and abrasive failure) for the β-TCP/Ch coatings is associated with the morphological surface evolution exhibited in the AFM results (Fig. 5) together with the evolution of the mechanical properties evidenced in Fig. 7 and Fig. 8.

3.6. Adhesion behavior

Scratch-test technique was carried out to measure the adherence strength of the β-TCP/Ch coatings. To identify the adhesion properties of the coatings, it is important to consider a lower critical load (L_{C1}). It is defined as the load where the first cracks occurred (cohesive failure) and the highest critical load (L_{C2}) where occurs the first delamination at the edge of scratch (adhesive failure) [46]. L_{C1} and L_{C2} values correspond to the tribological zones where the friction is independent on the applied load [47]. The critical load (L_{C1} and L_{C2}) values for all the β-TCP/Ch coatings are shown in Fig. 11, which shows the critical load values experimentally determined from the friction coefficient as a function of applied load.

From Fig. 11 it was possible to analyze the real adhesive response associated with the β-TCP/Ch coatings, hence, the curves of friction coefficient as a function of load showed that the values of L_{C1} are similar in Fig. 11a - d. However, for the coatings with higher percentages of chitosan (35% and 50%), the critical load associated with the cohesive failure is higher, as shown in Fig. 11e and f. On the other hand, the critical load is associated with the adhesive failure, which is closely related to the chitosan percentage. In this way, the friction coefficient curves as a function of load showed that L_{C2} increased when the chitosan percentage increased. Moreover, the improvement in the adhesion behavior of the β-TCP/Ch coatings could be related to the tribological analysis showed in Fig. 9 from pin-on-disk results. Similarly, the improvement in the mechanical behavior exhibited in Fig. 7 and Fig. 8, could be also associated to the changes in the crystal lattice arrangement studied in Fig. 1 and Fig. 2 and the evolution in the topography and morphological surface observed by SEM and AFM techniques, respectively.

As mentioned before, the chitosan percentage is influenced on the values of L_{C2}, Fig. 12 shows the L_{C2} curve as a function of chitosan percentage. This curve indicates that the adhesive critical load of the coatings increase by further increasing the chitosan percentage, in another word, a higher stress should be applied to reach the delamination of the coatings. From the data reported by other authors, it is possible to conclude that the tribological results were governed by the elastic-plastic properties of the β-TCP/Ch coatings and adhesion corresponding to the interface (β-TCP/Ch coatings-substrate) because the β-TCP/Ch systems have a relatively high elastic recovery (R%) values [47]. As can be seen in Fig. 8a, the critical load changes occur due to the increasing of plastic deformation resistance (H^3/E^2) [47] (showed in Fig. 8b), which generates opposition to indenter penetration producing an opposition to coating deformation. Thus, the last tribological and mechanical properties are related to a rhombohedral arrangement with the obtained results for all the coatings.

4. Conclusions

In this study, different types of β-TCP/Ch coatings were deposited via an electro-deposition method. It is shown that the preferential orientation for rhombohedral arrangement were (0018), (1118) and (0502) orientations for 2θ =(43.55°, 47.06° and 50.68°), respectively. From the SEM micrographs, it was possible to observe the topography changes on the surface coatings in relation with different chitosan percentages. These changes were associated with the results of the morphological analysis of β-TCP/Ch coatings performed by using AFM analysis, which showed the decrease of grain size and roughness as a function of chitosan percentage.

Different mechanical properties such as hardness were obtained for the β-TCP/Ch coatings. It was also determined that the elastic modulus (Er) and elastic recovery increased as function of increasing the chitosan percentage. These results were expected taking into account the changes in preferential peaks of XRD that suggested a deformation hardening.

The tribological behavior was studied, in which it was obtained low friction coefficient into the tribological system

(steel pin and β-TCP/Ch coatings) for all the coatings. This study suggested an improvement in tribological properties of the coatings evidencing an increase of adhesion resistance as function of chitosan increase. Therefore, the improvement in tribological behavior could be expected taking into account the improvement of the elastic-plastic behavior exposed by the β-TCP/Ch coatings by increasing the chitosan percentage.

From the SEM results it was possible to identify the wear mechanisms in each coating, (abrasive and adhesive wear) with failure by fatigue were evidenced by micrographs which are reduced when the chitosan percentage is increased. In this sense is possible to observe a decrease in the evidence of wear mechanisms due to the improvement in elastic-plastic behavior of the coatings, which open up new features for future of surgical implants.

Acknowledgments

This research was supported by the Universidad Militar Nueva Granada, Bogotá-Colombia project IMP-ING-1775 and the Excellence Center for Novel Materials (CENM) at Universidad del Valle in Colombia under Contract RC-043-2005 with Colciencias.

1. J.B. Brunski, in: B.D. Ratner, A.S. Hoffman, F.J. Schoen, and J.E. Lemons (Eds.), *Biomaterials Science an Introduction to Materials in Medicine*, 2nd ed., (Elsevier Academic Press, San Diego, 2004) p. 137.
2. B. Karim, J. Jean, D. Mainard, P. Elisabeth, and N. Patrick, *Biomaterials* **17** (1996) 491.
3. E. Salahinejad *et al.*, *PLoS ONE* **8** (2013) 1-8.
4. M. Mozafari *et al.*, *International Journal of Nanomedicine* **8** (2013) 1665-1672.
5. S.M. Naghib, M. Ansari, A, Pedram, F. Moztarzadeh, and A. Feizpour, M. Mozafari, *International Journal of Electrochemical Science* **7** (2012) 2890-2903.
6. E. Salahinejad *et al*., *Journal of Biomedical Nanotechnology* **9** (2013) 1327-35.
7. M.J. Cross, E.N. Parish, and J. Bone, *Joint Surg Br* **87** (2005) 1073-6.
8. T. Jinno, D.T. Davy, and V.M. Goldberg, *J. Arthroplasty.* **17** (2002) 902-9.
9. X. Pang, and I. Zhitomirsky, *Colloid and Interface Science*. **330** (2009) 323-329.
10. D. Peña, H. Estupiñan, H. Cordoba, and C. Vasquez, *Rev. Fac. Ing. Univ. Antioquia* (54) (2010) 15-23.
11. Y. Abe, T. Kokubo and T. Yamamuro, *Materials Science. Materials in Medicine* **1** (1990) 233.
12. L. Pighinelli and M. Kucharska, *Journal of Biomaterials and Nanobiotechnology* **4** (2013) 20-29.
13. S.-J. Ding, *Dental Materials Journal* **25** (2006) 706-712.
14. M. Kucharska, A. Niekraszewicz, M. Wisniewska-Wrona, E. Wesolowska and H. Struszczyk, *Progress on Chemistry and Application of Chitin and Its Derivatives*. **3** (2003) 69-72.
15. G.R. Bamwenda, K. Sayama, and H. Arakawa, *J. Photochem. Photobiol., A Chem.* **122** (1999) 175.
16. O. Bohnke, C. Bohnke, and G. Robert, *Solid State Ion*. **6** (1982) 121.
17. D. Davazoglou, A. Donnadieu, and A. Donnadicu, *Solar Energy Mat.* **71** (1988) 379.
18. E. Salahinejad, M.J. Hadianfard, D.D. Macdonald, M. Mozafari, D. Vashaee, and L. Tayebi, *Materials Letters* **88** (2012) 5-8.
19. R. Hurdich, *Electron Lett.* **11** (1975) 142.
20. K.D. Lee, *Thin Solid Films* **302** (1997) 84.
21. P.M.S. Monk, and L.S. Chester, *Electrochim. Acta* **38** (1993) 1521.
22. A.I. Inamdar, S.H. Mujawar, V. Ganesan and P.S. Patil, *Nanotechnol* **19** (2008) 325706.
23. E.M. Castro, H A. Estupiñan, and D.Y. Peña, *Scientia et Technica* **13** (2007) 36.
24. D.S. Metsger, M.R. Rieger, and D.W. Foreman, *J. Mater Sci Mater Med* **10** (1999) 9-17.
25. X. Guo, L. Lee, L.P. Law, H. Chow, R. Rosier, and C. Cheng, *J. Orthop. Res* **20** (2002) 740-746.
26. S.S. Banerjee, S. Tarafder, N.M. Davies, A. Bandyopadhyay, and S. Bose, *Acta Biomaterialia*. **6** (2010) 4167-4174.
27. E.T. den Braber, J.E. de Ruijter, and L.A. Ginsel, *Biomaterials* **17** (1996) 2037-2044.
28. M. Zhang, X.H. Li, Y.D. Gong, N.M. Zhao, and X.F. Zhang, *Biomaterials*. **23** (2002) 2641-2648.
29. R. Martínez H. Estupiñan, D. Peña, and P. Mohan, *Scientia et Technica.* **36** (2007) 36.
30. W.C. Oliver and G.M. Pharr, *Journal of Materials Research* **7-6** (1992) 1564-1583.
31. W. Jiawei, *Journal of Biomedical materials Research. Part. A.* **76** (2006) 503-511.
32. A. Tejada, C. Piña, S. Martínez, and G. Ávila, *Rev. Mex. Fis.* **5** (2004) 187-192.
33. G. Tomoaia, A. Mocanu, I. Vida-Simiti, N. Jumate, L. Dorel Bobos, and O. Soritau, M. Tomoaia-Cotisel, *Materials Science and Engineering: C*, **37** (2014) 37-47.
34. G.S. Kim, S.Y. Lee, and J.H. Hahn, *Surf. Coat. Technol.* **171** (2003) 91-95.
35. J. Zhang, W. Liu, V. Schnitzler, F. Tancret, and J. Bouler, *Acta Biomaterialia*. **10** (2014) 1035-1049.
36. G. Cabrera, J.C. Caicedo, C. Amaya, L. Yate, J. Muñoz Saldaña, and P. Prieto, *Materials Chemistry and Physics.* **125** (2011) 576-586.

37. V.V. Hajek, K. Rusnak, J. Vlcek, L. Martinu and H.M. Hawthorne, *Wear* **213** (1997) 80-86.

38. J.C. Caicedo *et al*., *Applied Surface Science.* **256** (2010) 5898-5904.

39. G.S. Kim, S.Y. Lee, and J.H. Hahn, *Surface and Coatings Technology.* **171** (2002) 91-95.

40. P.J. Burnett and D.S. Rickerby, *Thin Solid Films.* **154** (1987) 403-416.

41. J.C. Caicedo, G. Bejarano, M.E. Gómez, P. Prieto, C. Cortéz, and J. Muñoz, *Phys. Stat. Sol.* **4** (2007) 4127-4133.

42. J. Romero, A. Lousa, J. Esteve, and E. Martínez, *Applied Physics A: Materials Science & Processing.* **77** (2003) 419-427.

43. J.F. Archard. *Journal of Applied Physics.* **24** (1953) 981.

44. P. Nledengvist and S. Hogmark, *Tribology International.* **30** (1997) 507-516.

45. L. Ipaz, J.C. Caicedo, J. Esteve, F.J. Espinoza-Beltran, and G. Zambrano, *Applied Surface Science* **258** (2012) 3805- 3814.

46. S.J. Bull, D.S. Rickerby, A. Matthews, A. Leyland, A.R. Pace, and J. Valli, *Surf. Coat. Technol.* **36** (1988) 503-517.

47. J.M Lackner, L. Major, and M. Kot, *Bull. Pol. Ac.: Tech.* **59** (2011) 343-355.